

# *ForEdgeClim*

Emma Van de Walle - Q-ForestLab

May 2025



In this report an overview of the model *ForEdgeClim* is written down. *ForEdgeClim* is a process-based microclimate model that is initially written to simulate microclimate gradients along transect lines from a forest's core towards its edge.

The model follows a mechanistic approach to microclimate modelling, grounded on the principle of energy conservation. Semi-opaque surfaces in the environment, such as the canopy and the ground, absorb solar radiation while simultaneously emitting thermal radiation. These surfaces also exchange sensible heat with the air and experience latent heat fluxes (here, cooling by evapotranspiration). Additionally, the ground stores and releases energy, contributing to the overall energy balance.

Since each component of the energy budget depends on temperature, they are all included in an iterative loop until energy balance convergence is reached and this for a steady state, single moment in time. [Note: this convergence is pursued for the surface (i.e., forest structural) temperature. Air and soil surface temperature are modelled as well, but are updated by the updated surface temperature. Therefore, there is no convergence criterion for air and soil surface temperature. (See further for more explanation.)]

The assumption of a steady state condition is valid here because our objective is to model temperature between consecutive hourly time steps, and thermal equilibrium is reached much faster than the hourly time step we apply. There is therefore no temporary heat accumulation or delayed temperature response. We could make the model dynamic, which could be interesting for studying temporal dynamics related to heat storage or soil dynamics. However, our current focus is on modelling temperature through processes such as radiation, latent heat, sensible heat, and ground heat flux, all of which reach equilibrium more quickly than the hourly time step.

The use of an iterative loop is necessary because no closed-form mathematical solution exists for the energy budget equations. All processes in the microclimate model continuously influence each other, and only through repeated updates can a stable and physically realistic temperature distribution

be achieved. One of the complex interdependencies is for example the relationship between surface heating and sensible heat exchange.

The model starts by simulating shortwave radiative transfer (RTM) that calculates shortwave radiation in two directions: vertical and lateral. The RTM is therefore two-dimensional. Next, it attempts to close the energy balance by reducing the energy balance closure error to less than  $E_{bal}$ , an equilibrium criterion variable (e.g.  $1 \text{ W/m}^2$ ). This equation (eq. 1) balances the net radiation ( $R_n$ ), sensible heat flux ( $H$ ), latent heat flux ( $LE$ ), and ground heat flux ( $G$ ) for the forest structure. Ground heat flux ( $G$ ) is 0 everywhere except for the soil. It is (currently) only used to simulate soil surface temperature, which in turn influences air temperature. Net radiation consists of both shortwave and longwave radiation in 2D. Sensible heat flux is calculated in 3D, whereas latent heat flux and ground heat flux are calculated in 1D (vertically). The processes are carried out between voxels in 3D. Each voxel contains a density value, determined from terrestrial laser scanning (TLS) data to account for the forest structure.

$$E_{bal} = R_n - H - LE - G = 0 \quad (1)$$

## Modelling temperatures

As mentioned before, *ForEdgeClim* models three temperature values. First and foremost, the surface temperature  $T_f$  is modelled. This temperature represents the temperature of the forest surface structures within the voxel grid, i.e., leaves, branches and stems. In the model, Newton's method is applied, as described above, to update the surface temperature between successive iteration steps.

In addition to surface temperature, both air temperature  $T_{air}$  and soil surface temperature  $T_s$  are modelled. Air temperature represents the temperature of the air within each voxel. Since each voxel has a certain density value representing the structure, the remaining density (1 - density) represents the air. Soil surface temperature is a single-layer temperature, effectively representing the ground surface temperature. Below, further explanation is provided on how air and soil surface temperature are modelled.

### Air temperature

Modelling air temperature is done via a linearisation, similar to the approach used in the microclimate model *microclimf* by Ilya Maclean. This method is mostly valid when there are small temperature differences between air temperature and surface temperature, when there is sufficient air streaming, when the net radiation or the humidity is not extreme and when the forest structure is quite homogeneous.

Air temperature is derived as shown in eq. 2. In this equation  $w$  refers to weight,  $g$  to convection and  $T$  to temperature. The subscript  $m$  refers to macroenvironment,  $s$  to soil and  $f$  to forest surface.  $mX$  and  $mZ$  further refer to the macroenvironment along the X-axis (lateral) and the Z-axis (vertical), respectively.

The weights  $w$  are defined as exponential weightings of the boundary distances. All definitions of  $w$  have the same structure, an example for  $w_s$  is given in eq. 3. Here,  $d_s$  is the distance to the forest soil surface and  $\alpha_s$  is defined in eq. 4. In eq. 4,  $i_s$  is the 'distance of influence'.  $i_s$  is defined as the distance over which the influence of soil surface temperature on air temperature is reduced by 50%. Exponential weighting is well-suited for microclimate modelling as it naturally represents the gradual decline in influence with distance, aligning with physical heat transfer principles. It ensures smooth transitions between temperature sources, accommodates varying spatial scales, and integrates

well with convection and conduction processes. Additionally, it prevents unrealistic temperature fluctuations and maintains numerical stability.

The convections  $g$  and the distances of influence  $i$  are input parameters and  $T_f$  is the to be modelled forest surface temperature. If a voxel does not contain forest structure (and therefore has no  $T_f$ ), the average surface temperature of the corresponding X-, Y- and Z-planes is used.

$$T_{air} = \frac{(w_{mX} + w_{mZ}) \cdot g_m \cdot T_m + w_s \cdot g_s \cdot T_s + w_f \cdot g_f \cdot T_f}{(w_{mX} + w_{mZ}) \cdot g_m + w_s \cdot g_s + w_f \cdot g_f} \quad (2)$$

$$w_s = e^{\alpha_s \cdot d_s} \quad (3)$$

$$\alpha_s = \log(0.5/i_s) \quad (4)$$

## Soil surface temperature

The soil surface temperature ( $T_s$ ) is modelled using the heat conduction equation (Fourier's law) in 1D (see eq. 5).  $T_{soil}$  is the mean observed soil temperature at 20 locations within the forest transect, measured at a depth of 6cm. This value is assumed to be stable over a time bin of around 6h.  $z$  is the depth at which this stable temperature is measured, i.e., 6cm,  $G$  is the ground heat flux and  $k_s$  the thermal conductance of the soil.  $G$  is explained further down.

$$T_s = T_{soil} + \frac{G \cdot z}{k_s} \quad (5)$$

## Radiative transfer model

The radiative processes are simulated in 2D (vertical and lateral) and use the two-stream radiative transfer model, based on the version also used in the *ED 2.2* model. (See the report [Two-stream Radiative Transfer Model of ED 2.2](#) for a detailed description of the model.)

In short, for the shortwave RTM, the model simulates multi-scatter radiative transfer along a single column or row, where direct and diffuse sunlight interact with a layered structure containing density values. Direct beam radiation ( $I_b^\downarrow$ ) is represented by an exponential decaying process, and the RTM solves for diffuse upward and downward radiation ( $I^\downarrow$  and  $I^\uparrow$ ) in each canopy layer using a linear matrix equation. Equations 6, 7 and 8 present the equations for the direct and diffuse radiation components. Table 2 includes and explains the parameters used in these equations.

$$\frac{dI_b^\downarrow}{dx} = -K_b I_b^\downarrow \quad (6)$$

$$\frac{dI^\downarrow}{dx} = -[1 - (1 - \beta)\omega]K_d I^\downarrow + \beta\omega K_d I^\uparrow + (1 - \beta_0)\omega K_b I_{sky,b}^\downarrow e^{-K_b x} \quad (7)$$

$$\frac{dI^\uparrow}{dx} = [1 - (1 - \beta)\omega]K_d I^\uparrow - \beta\omega K_d I^\downarrow - \beta_0\omega K_b I_{sky,b}^\downarrow e^{-K_b x} \quad (8)$$

The choice of values for the parameters in table 2 is not random. For example, in temperate forests, direct sunlight is significantly weakened by the presence of leaves, branches, and other structures that lie directly in the light path. Values for  $K_b$  in the vertical direction of around 0.90 correspond to the shading and absorption by dense canopies. Diffuse sunlight is less strongly attenuated because it comes from multiple directions and some of it can penetrate through small openings in the canopy. This results in a lower attenuation coefficient. The attenuation coefficients are, in principle, season-dependent; for instance, in winter, the attenuation coefficient can be lower due to the absence of leaves.

Lateral attenuation coefficients are lower because light travelling horizontally passes through a shorter path within the tree structure, often encountering fewer obstacles.

The parameters used in eq. 6, 7 and 8, along with the values of direct and diffuse solar radiation from the above canopy and the ground reflectance ( $\omega_g$ ), serve as input parameters for the shortwave two-stream RTM model.

This model is a 'single-column' model. To achieve a 2D RTM for our 3D grid, this model is applied to every vertical column (fixed XY) and every horizontal row (fixed YZ).

## Process 1 | Net radiation $R_n$

Net radiation is described in eq. 9 and consists of three terms derived from the shortwave RTM ( $I_b^\downarrow$ ,  $I^\downarrow$  and  $I^\uparrow$ ), as well as two terms representing incoming and outgoing longwave radiation ( $L^\downarrow$  and  $L^\uparrow$ ). Both longwave radiative terms are described using an analogous two-stream RTM model as described above, for the shortwave radiation. Yet, here, the direct beam radiation terms are removed, and a source of thermally emitted radiation is added. The equations governing the longwave terms are given in eq. 10 and eq. 11. In those equations,  $\epsilon_f$  and  $\sigma$  represent the forest emissivity and the Stephan-Boltzmann constant, respectively. All other parameters are similar as in eq. 7 and 8. The downward longwave radiation at the top of the canopy ( $L_{sky}^\downarrow$ ) is an input driver.

$$R_n = I^\downarrow - I^\uparrow + I_b^\downarrow + L^\downarrow - L^\uparrow \quad (9)$$

$$\frac{dL^\downarrow}{dx} = -[1 - (1 - \beta)\omega]K_dL^\downarrow + \beta\omega K_dL^\uparrow + \epsilon_f\sigma T_f^4(1 - \beta)\omega K_d \quad (10)$$

$$\frac{dL^\uparrow}{dx} = [1 - (1 - \beta)\omega]K_dL^\uparrow - \beta\omega K_dL^\downarrow + \epsilon_f\sigma T_f^4(1 - \beta)\omega K_d \quad (11)$$

## Process 2 | Ground heat flux $G$

Ground heat flux is modelled as a percentage ( $p$ ) of the net radiation at ground level and is given in eq. 12 (ref. *SCOPE 2.0* model). Here  $\rho$  is the forest density (in the layer just above the ground).

$$G = p \cdot (1 - \rho) \cdot R_n \quad (12)$$

## Process 3 | Sensible heat flux $H$

A surface heated by solar radiation transfers some of this heat to the surrounding air. According to the laws of energy conservation, the air absorbs this heat. This process is known as sensible heat exchange. In *ForEdgeClim* sensible heat exchange is conducted in 3D and simulates 1, heat diffusion ( $D$ ) between the air of adjacent neighbouring voxels using the formula for heat transfer by diffusion (Fourier's law of heat conduction) (eq. 13 and 14) and 2, heat convection (actual sensible heat exchange) from the forest surface to the surrounding air (eq. 15). At the edges of the grid, there is also a transfer of heat with the macroenvironment and forest soil surface.

In eq. 13,  $h$  is the thermal diffusion coefficient of air,  $A$  the surface area of one voxel face and  $\Delta T_{air}$  the difference in air temperature between neighbouring voxels. In eq. 14,  $c_p$  is the specific heat of air,  $\rho_{air}$  the density of air and  $V$  the voxel volume.

In eq. 15,  $g_f$  is the forest convection.

$$D = h \cdot A \cdot \Delta T_{air} \quad (13)$$

$$T_{air-new} = T_{air-old} - \frac{D}{c_p \cdot \rho_{air} \cdot V} \quad (14)$$

$$H = \rho \cdot g_f \cdot (T_f - T_{air}) \quad (15)$$

## Process 4 | Latent heat flux $LE$

Latent heat flux is modelled using the empirical Priestley-Taylor method (eq. 16). This is a simplified version of the Penman-Monteith equation that simulates the potential evapotranspiration and where all aerodynamic variables are encapsulated in a single parameter,  $\alpha$ , the Priestley-Taylor coefficient. In this equation, it is assumed that the aerodynamic term (the advective component) is negligible. As a result, evapotranspiration can be calculated based on the available net radiation energy and the psychrometric constant. It performs well under specific climatic and environmental conditions. These conditions include negligible advective processes, surfaces with unlimited water availability, radiation being the dominant factor for evaporation, and relatively stable atmospheric conditions (i.e., no extreme wind, pressure, or humidity variations).

$$LE = \rho \cdot \alpha \cdot R_n \cdot \frac{s(T_{fc})}{s(T_{fc}) + \gamma} \quad (16)$$

In eq. 16,  $\gamma$  is the psychrometric constant and  $s$  represents the slope of the saturation pressure curve in  $kPa/K$  and is further defined in eq. 17.  $T_{fc}$  is the forest structural temperature expressed in  $^{\circ}C$ . This in contrast with  $T_f$ , which is expressed in K.

$$s(T_{fc}) = 4098 \cdot \frac{e_s(T_{fc})}{(T_{fc} + 237.3)^2} \quad (17)$$

In eq. 17,  $e_s$  is the saturated vapor pressure. It is calculated using the empirical formula by Tetens (see eq. 18). The formula by Tetens is an empirical approximation of the Clausius-Clapeyron equation and works well for temperatures between  $-40^{\circ}C$  and  $50^{\circ}C$ .

$$e_s(T_{fc}) = 0.6018 \cdot \exp\left(\frac{17.27 \cdot T_{fc}}{T_{fc} + 237.3}\right) \quad (18)$$

## Solving the energy balance

Within the iterative loop to converge the energy balance per voxel, and therefore for the entire system, net radiation, sensible heat flux, latent heat flux, ground heat flux, air temperature and soil surface temperature are updated by an updated surface temperature.

Based on the *SCOPE 2.0* model, Newton's method is used to update surface temperature values between successive iteration steps. This method utilizes the energy balance closure error ( $E_{bal}$ ) and its derivative with respect to forest temperature (see eq. 19). In this equation,  $W$  is a weighting for the step size.

$$T_{f-new} = T_{f-old} - W \cdot \frac{E_{bal}(T_f)}{\frac{\delta E_{bal}(T_f)}{\delta T_f}} \quad (19)$$

The derivative of the energy balance closure error to the forest temperature can further be written as:  
(Remark that there is no derivative of G because G is only calculated for the soil surface and not for the structural surface of the forest.)

$$\frac{\delta E_{bal}(T_f)}{\delta T_f} = \frac{\delta R_n(T_f)}{\delta T_f} - \frac{\delta H(T_f)}{\delta T_f} - \frac{\delta LE(T_f)}{\delta T_f} \quad (20)$$

And from the formulas in the sections above, it follows that eq. 20 can be further expanded as:

$$\frac{\delta E_{bal}(T_f)}{\delta T_f} = -4 \cdot e_f \cdot \sigma \cdot T_f^3 - \rho \cdot g_f - \rho \cdot \alpha \cdot (-4 \cdot e_f \cdot \sigma \cdot T_f^3) \cdot \frac{s}{s + \gamma} + \rho \cdot \alpha \cdot R_n \cdot \frac{dF(T_f)}{dT_f} \quad (21)$$

with

$$\frac{dF(T_{fc})}{dT_{fc}} = \frac{\frac{ds(T_{fc})}{dT_{fc}} \cdot (s + \gamma) - s \cdot \frac{ds(T_{fc})}{dT_{fc}}}{(s + \gamma)^2} \quad (22)$$

and

$$\frac{ds(T_{fc})}{dT_{fc}} = \frac{4098 \cdot \frac{de_s(T_{fc})}{dT_{fc}} \cdot (T_{fc} + 237.2)^2 - 2 \cdot (T_{fc} + 237.3) \cdot 4098 \cdot e_s(T_{fc})}{(T_{fc} + 237.3)^4} \quad (23)$$

and

$$\frac{de_s(T_{fc})}{dT_{fc}} = 0.6108 \cdot \exp\left(\frac{17.27 \cdot T_{fc}}{T_{fc} + 237.3}\right) \cdot \frac{(T_{fc} + 237.3) \cdot 17.27 - 17.27 \cdot T_{fc}}{(T_{fc} + 237.3)^2} \quad (24)$$

## Numerical approach

*ForEdgeClim* employs a grid-based numerical approach to simulate microclimate temperature and energy exchange in fragmented forests. Given the structured nature of the 3D voxel-based representation of the forest, a grid-based method is a logical choice, ensuring spatially explicit calculations and allowing for efficient computation of radiative and heat transfer processes.

The model integrates two numerical methods: the Finite Difference Method (FDM) and the Finite Volume Method (FVM). FDM is utilised for air-to-air convective heat transfer, where temperature gradients are approximated using finite difference schemes. This allows for an efficient discretisation of heat diffusion processes within the voxel grid. Meanwhile, FVM is applied to solve the energy balance equation, ensuring conservation of energy fluxes at the voxel scale. FVM is particularly advantageous in this context as it explicitly accounts for energy exchange between adjacent voxels, which is essential for accurately modelling the interactions between forest structure, air, and soil surface.

The choice of a grid-based approach over particle methods (like Monte Carlo methods) or mesh-based methods is motivated by the structured nature of forest transects in the model. A voxel-based discretisation aligns well with available 3D structural data, such as LiDAR-derived forest density maps, allowing for direct incorporation of empirical data. Furthermore, grid-based methods facilitate efficient coupling of radiative transfer, heat exchange, and evapotranspiration processes within a unified computational framework. This hybrid FDM-FVM approach balances computational efficiency with physical accuracy, making it well-suited for simulating spatially heterogeneous microclimates in complex forested environments.

# Input drivers, (physical) constants, model parameters, and prognostic variables

An overview of the input drivers, (physical) constants, model parameters and prognostic variables is respectively given in table 3, 4, 2 and 5.

If a table contains the column 'submodel', this refers to the process(es) to which the variable contributes. Submodels can be shortwave RTM (SW RTM), longwave RTM (LW RTM), sensible heat flux (H), latent heat flux (LE), ground heat flux (G), air temperature ( $T_{air}$ ), and soil surface temperature ( $T_s$ ).

The several model parameters can be tweaked to calibrate and validate our model.

## Some first results

The structure grid used in the simulation below is the TLS scan taken from the transect in Gontrode forest in July 2023. An illustration can be found in figure 1 in 2D. The forest edge is located on the right side, in the east, at the maximum X-position. We assume that there is more forest to the north, west, and south. Hence, in the 2D RTM, radiation enters from above and from the right side. The density of each voxel is normalised and ranges between 0 and 1. In the transect, we observe a gap around the  $X = 50\text{m}$  position. This is due to ash dieback, caused by a chronic fungal disease affecting ash trees in Europe, characterised by leaf loss and crown dieback in infected trees. The transect consists mainly of ash trees between  $X = 0$  and  $X = 50$ , while beyond  $X = 50$ , it is predominantly composed of beech and oak trees. In the figure, we also see a higher structure to the right of the gap. This is the flux tower located within the transect. We furthermore observe a higher density in the upper right part of the gap. Here, a healthy oak is taking advantage of the ash dieback to expand its canopy.

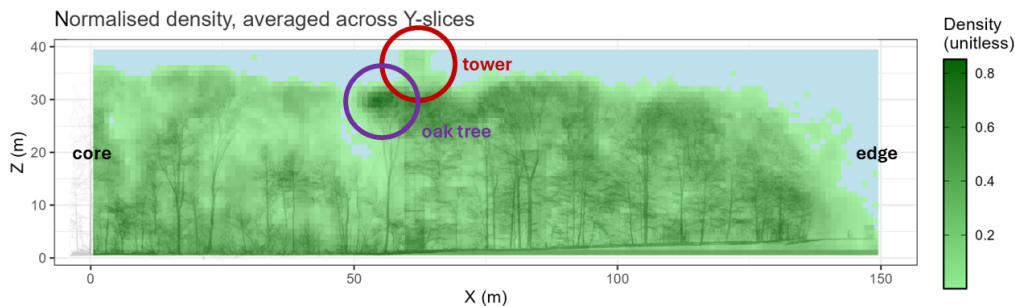


Figure 1: Cross-sectional density plot of 3D grid in 2D

Figure 2 shows the digital terrain model derived from the TLS scans. Along the western side, we see a small river running from north to south, while on the eastern side, there is a road. The terrain slopes upward from west to east, meaning the road is at a higher elevation than the river. The parallel lines are furrows, a common technique used to improve drainage in wet forests. These furrows are very old and were likely established before the 1650s. Trees could be planted on the elevated, and therefore drier, ridges.

In the simulation discussed below, the microclimate forest surface temperature, air temperature and soil surface temperature are modelled for the location Gontrode in Belgium on July 8, 2023, at 12:00:00 UTC, the hottest day of that year. Input drivers and model parameters similar to the ones mentioned in tables 3 and 2 are used in this simulation.

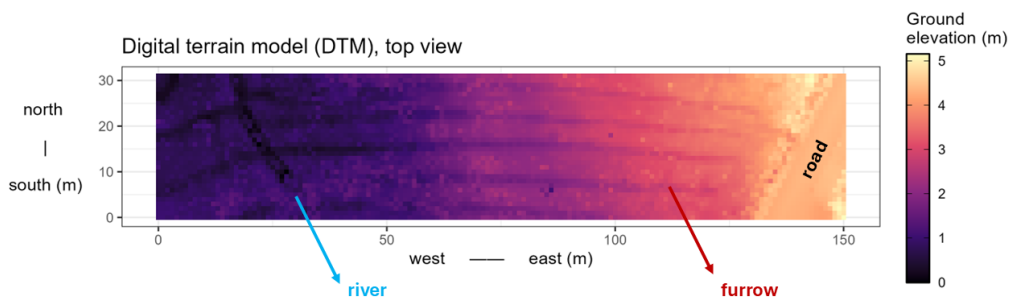


Figure 2

Figure 3 shows the shortwave direct beam downward radiation for both the vertical and lateral direction (averaged over Y-slices). We observe that light can penetrate deep within the forest gap and is attenuated quite fast in denser canopy areas.

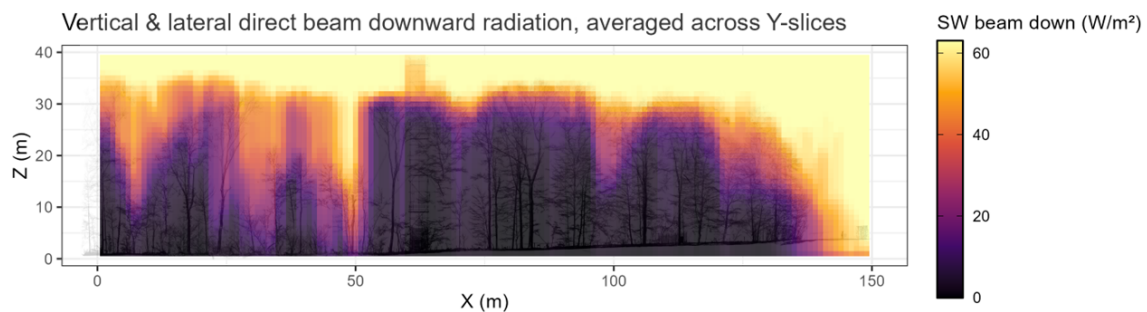


Figure 3

In figure 4, you can see the air temperature averaged over Y-slices along the transect. We see that the macrotemperature outside the forest transect is around  $31^\circ\text{C}$ , as expected, since the macrotemperature input driver is set to  $31.4^\circ\text{C}$ . At the top of the canopy, we observe warming due to the leaves absorbing and re-emitting radiation. Beneath the canopy, along the ground, there is a clear cooling effect.

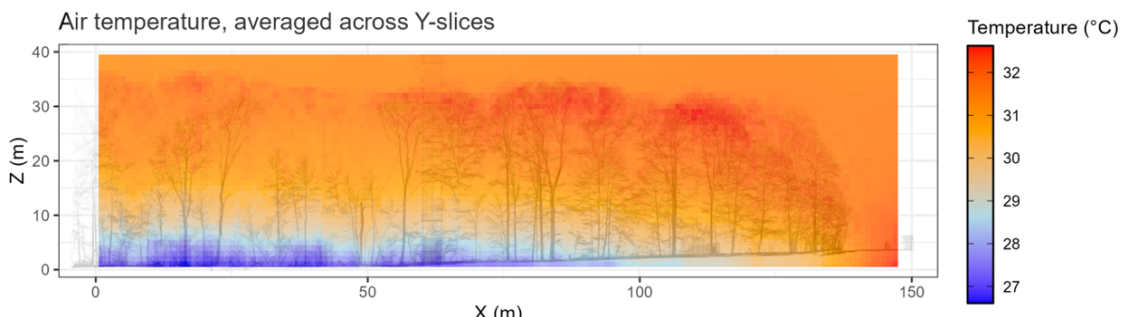


Figure 4

Figure 5 displays the surface temperature. Here too, we observe higher temperatures at the top of the canopy and lower temperatures deeper in the forest and along the ground. Compared to the air temperature shown in figure 4, we observe that temperatures in the canopy are higher (up to  $35^\circ\text{C}$ ). The temperature distribution of the forest surface temperature is wider compared to the one of air temperature.

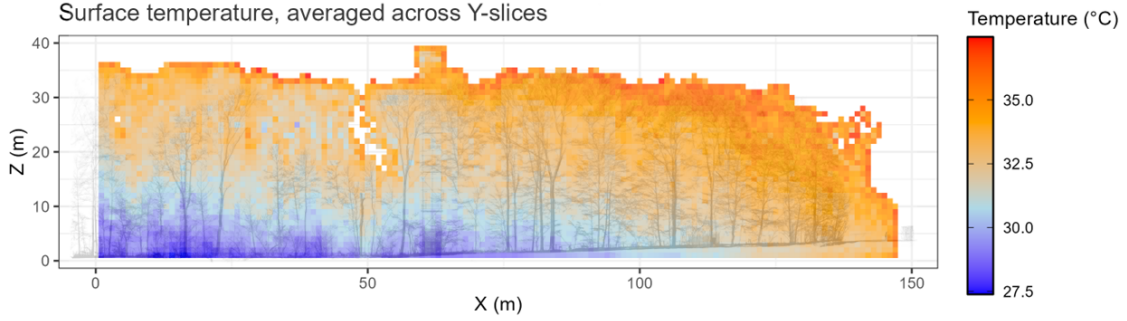


Figure 5

Figure 6 shows the soil surface temperature, just below the lowest Z-grid layer. Here, we observe that the highest temperatures are located at the forest edge, where a road is present. As we move further into the forest, we see a cooling effect, with a slight warming occurring where the forest gap is located.

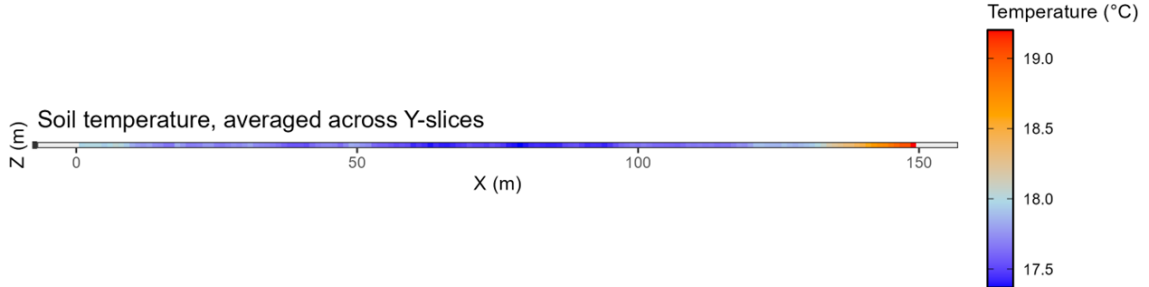


Figure 6

If we then plot the air temperature for the voxels at 1m height along the transect (not averaged over Y-slices, but for the central Y-value, representing the central transect line), we obtain figure 7. Here, we compare the model output in blue with TOMST sensor observations in green. We mainly observe a decrease in temperature from the edge to the interior. This is due to, among other factors, the shading capabilities of the forest, which ensure that radiative heating primarily occurs in the top canopy rather than in the lower structures. Additionally, the heat transfer buffering effect of the forest structure plays a role, bringing warm macroair in along the edge but preventing it from being conducted all the way to the core.

In addition to the horizontal gradient shown in figure 7, figure 8 presents the vertical gradient. The latter is modelled and simulated for the central vertical line of the transect grid and represents conditions at 12h PM as well. We observe that temperature increases with increasing height. Just at the top of the canopy, the temperature reaches its maximum, before decreasing again above it.

*ForEdgeClim* also produces plots that display the various fluxes. An example of the net radiation flux is shown in figure 9. Here, we see that most radiation is absorbed at the top of the canopy, along the forest edge, and within the gap.

Figure 10 shows the air temperature during a summer night. Compared to figure 7, there are fewer fluctuations, with the most prominent feature being the steady and colder temperature from the forest edge to the core. This corresponds to the expected weaker temperature differences between the forest and the macroenvironment during colder periods.

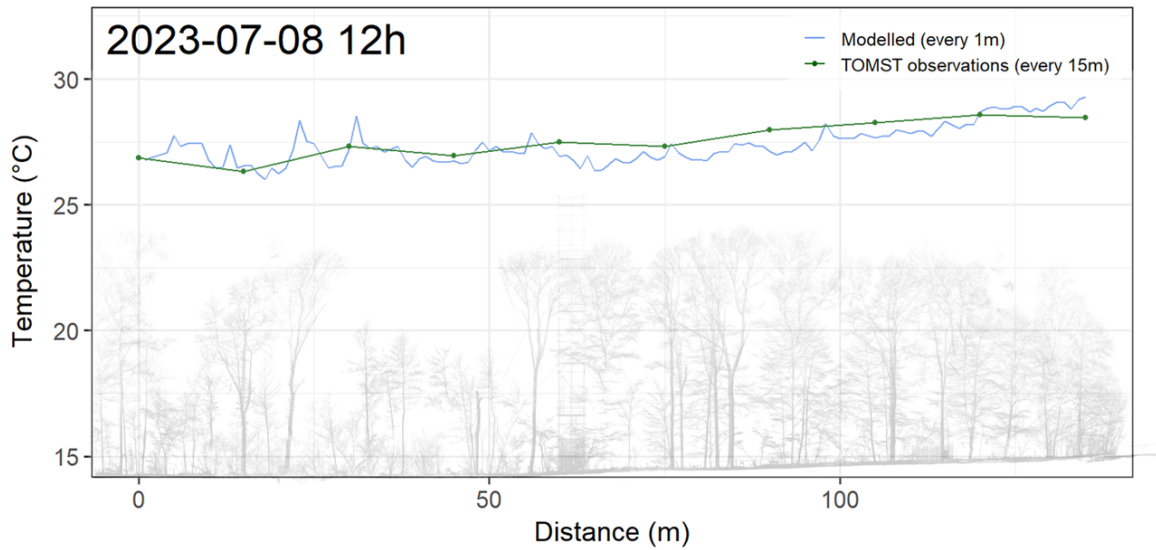


Figure 7: Modelled and observed air temperature at 1m height during a summer day

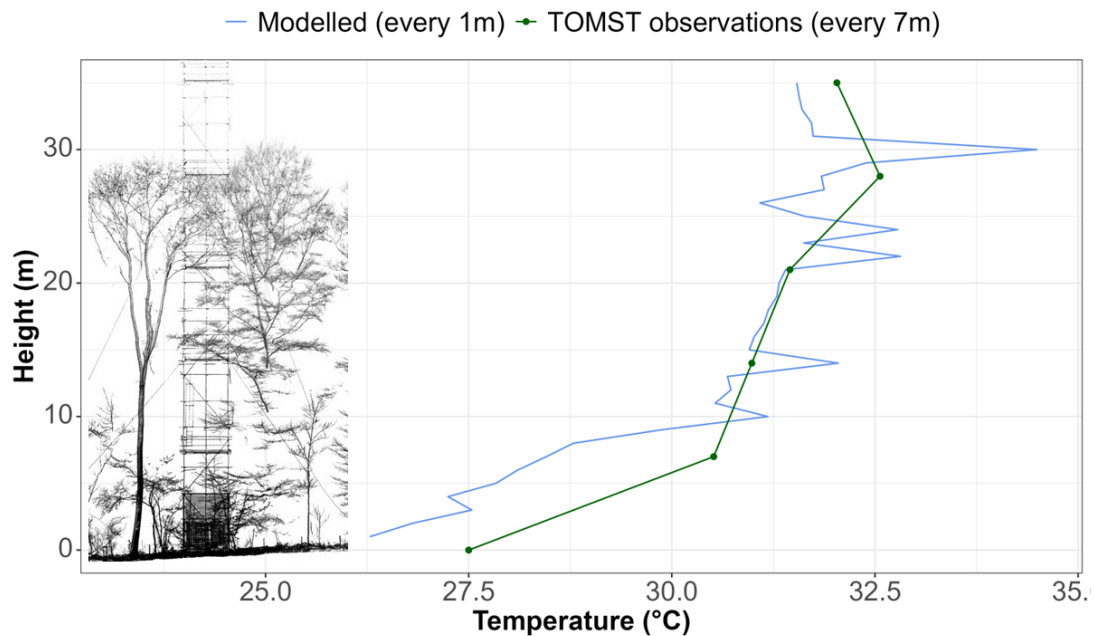


Figure 8: Modelled and observed air temperature along the vertical tower during a summer day

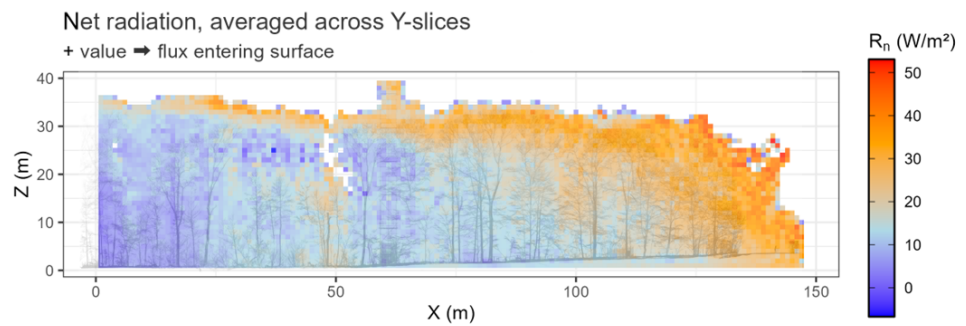


Figure 9

In Figure 11, we observe an even clearer gradient during the morning of 8 July 2023. Around

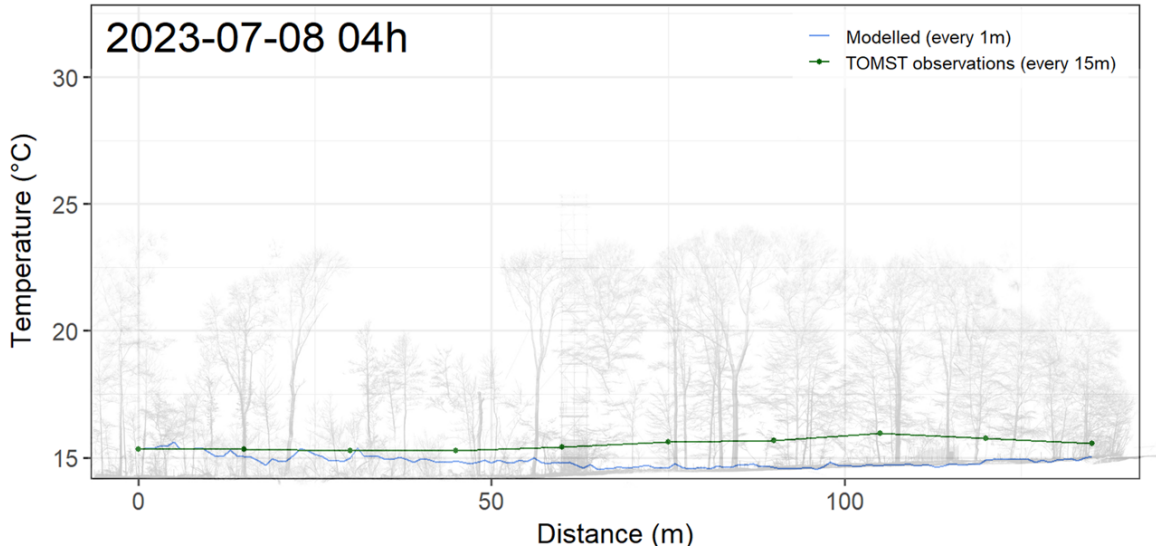


Figure 10: Modelled and observed air temperature at 1m height during a summer night

this time, the sun rises and a relatively large amount of lateral radiation enters along the forest edge (eastern side). We can therefore clearly see the effect of lateral radiation in creating a temperature gradient, demonstrating that it is important to include this process in a microclimate model if we wish to account for edge effects. Moreover, there is likely a larger difference in temperature between the area outside and inside the forest during the morning. In the afternoon, for example, the forest has already warmed up, resulting in a less pronounced gradient, but higher absolute temperature values (as seen in figure 7).

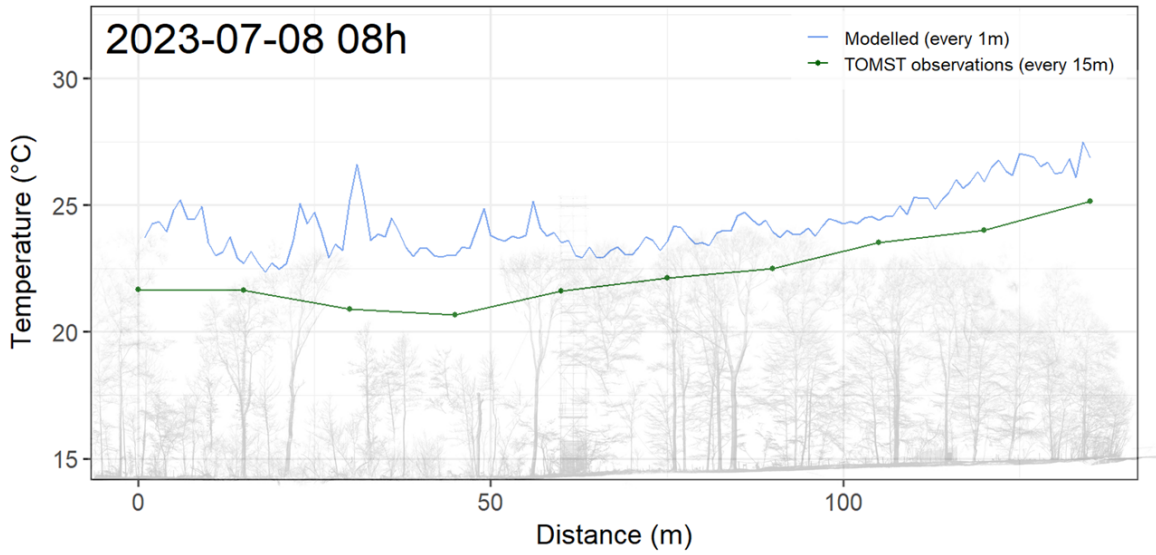


Figure 11: Modelled and observed air temperature at 1m height during a summer morning

If we plot a time series of eight time points on the same warm summer day, 8 July 2023, we obtain Figure 12. Both the model output and the TOMST observations, as well as the forest core and forest edge, are compared. We observe that the temperature near the edge leads that of the core, and that the amplitude (minimum and maximum) of the temperature fluctuations is also greater at the edge than in the core.

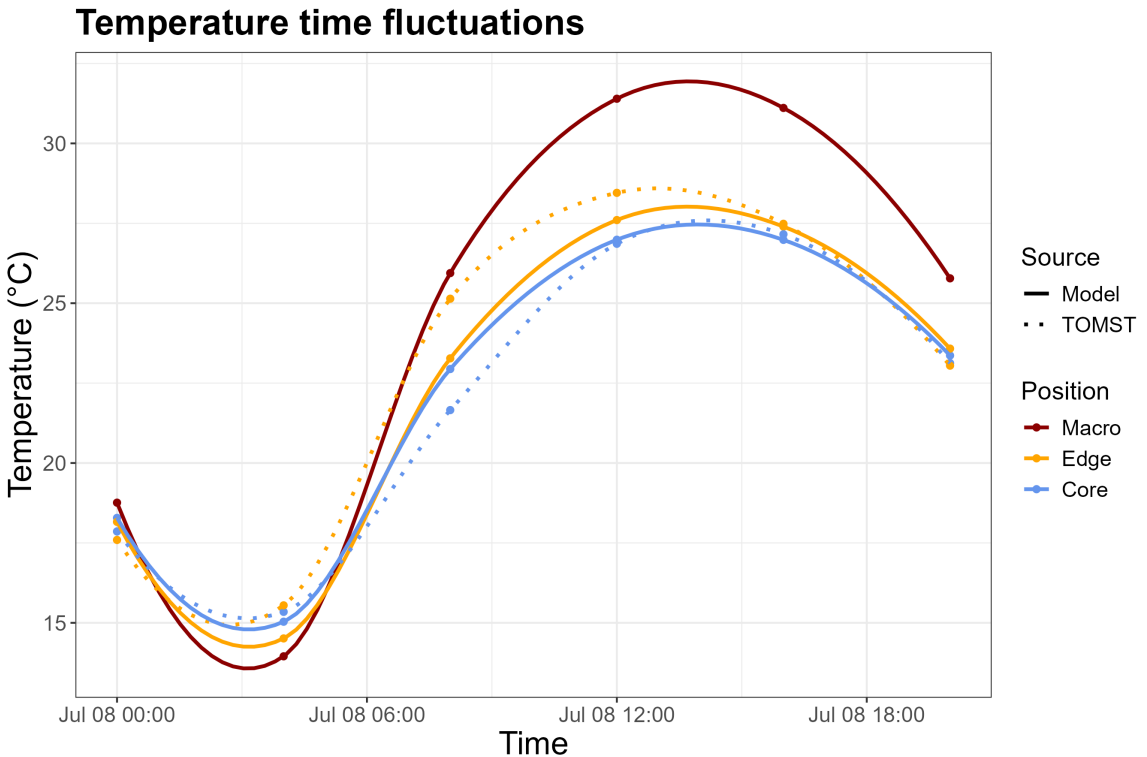


Figure 12: Modelled vs observed and core vs edge air temperature at 1m height during a summer day

## Sensitivity Analysis

As type of sensitivity analysis, we opted for a Sobol analysis (see subsection below for more information on Sobol analysis). We carried this out for four specific months representing the four seasons. Therefore, we selected January (winter), April (spring), July (summer), and October (autumn). Since we wanted to extract a complete time series of incoming radiation from our observations for each month, the years in which we performed the Sobol analyses differ: January 2025, April 2024, July 2023, and October 2024.

For each of these months, we identified the day with the best balance between high direct solar radiation and minimal fluctuations in direct solar input. We chose the day with both a high average value and a low standard deviation. For January, this was the 27th; for April, the 23rd; for July, the 7th; and for October, the 5th. The decision to select the day with the best balance between average direct sunlight and fluctuations in direct sunlight was necessary because our aim with the Sobol analysis is to study the effect of various model parameters on the forest's buffering capacity, and most buffering occurs under high direct solar radiation conditions.

For each of these four sunniest days, we conducted a Sobol analysis for three distinct time points: in the morning, in the afternoon, and during the night. These time points were selected based on the number of daylight hours in each season. The morning was defined as approximately one hour after sunrise (the onset of warming); the afternoon as the period just after solar noon (maximum temperature); and the night-time was consistently set at 03h00, as this hour is representative of the night across all seasons. Including the morning time point can be particularly insightful, as the sun rises in the east and the edge side of the forest is located on the eastern side. By focusing on this morning period in the Sobol analysis, we can examine whether the influence of the parameters changes when lateral radiation penetrates the forest. This allows us to better analyse the temperature gradient along the

transect within the Sobol framework. Table 1 shows the exact time points used. These time points are in European local time, meaning they follow UTC+2 (daylight saving time) between the last Sunday in March and the last Sunday in October, and UTC+1 (standard time) between the last Sunday in October and the last Sunday in March.

Table 1: Time points per season

Season	Month	Chosen day	Morning ☀	Afternoon ☀	Night ⚡
winter	January	27/01/2025	09h00	13h00	03h00
spring	April	23/04/2024	08h00	14h00	03h00
summer	July	07/07/2023	07h00	14h00	03h00
autumn	October	05/10/2024	09h00	13h00	03h00

After performing the Sobol analysis for each specific season and time point, the Sobol indices were determined for three types of metrics, also referred to as predictor variables. This resulted in  $4 \times 3 \times 3 = 36$  'Quantities of Interest', i.e. the number of seasons  $\times$  number of time points  $\times$  number of predictor variables. The predictor variables considered were the mean temperature, the standard deviation of the temperature, and the temperature gradient, all along the transect at a height of 1 meter.

## Sobol analysis

The Sobol analysis is a global sensitivity analysis technique. It quantifies how much each model parameter contributes to the variance in a model's output, i.e. a predictor variable.

There are two main types of indices:

### First-order (= direct-effect) Sobol index ( $S$ )

$$S_i = \frac{Var(\mathbb{E}[Y|X_i])}{Var(Y)} \quad (25)$$

$S_i$  measures the proportion of the total variance in the model output  $Y$  that is explained by variation in parameter  $X_i$  alone, while all other parameters are held constant. It therefore captures the direct influence of parameter  $X_i$  on the output.

### Total-effect Sobol index ( $T$ )

$$T_i = 1 - \frac{Var(\mathbb{E}[Y|X_{\sim i}])}{Var(Y)} \quad (26)$$

with  $X_{\sim i}$  all parameters except  $X_i$ .  $T_i$  measures the total proportion of variance in  $Y$  that is explained by the direct influence of  $X_i$  + all interactions in which  $X_i$  is involved. It therefore answers the question: how important is  $X_i$ , including all its combinations with other parameters?

This analysis is probabilistic: you assign each of your model parameters an uncertainty distribution (for example, uniform between a minimum and maximum), and then sample from those using Monte Carlo or Quasi-Monte Carlo methods. We use the stratified sampling technique of Latin Hypercube Sampling from uniform parameter distributions and used 400 parameter sampling sets. For each model parameter, typical value ranges were identified from the literature. Table 2 shows the typical value ranges ( $U(min, max)$ ).

## Final remarks

The *ForEdgeClim* model, as described in this report, aims to simulate microclimate/ -temperature in a (temperate) forest in a physically realistic manner, given macroinput drivers and forest structure. To achieve this, key contributing processes were identified and considered in terms of how they could be modelled in a physically accurate way. When selecting processes and their mathematical implementation, a balance was sought between detail and relevance.

*ForEdgeClim* is therefore not an extremely detailed microclimate model that accounts for all microclimatic ecosystem processes. However, the model currently appears to generate physically realistic output. In future versions, processes such as a more detailed soil heat flux, (lateral) wind, and hydrological processes seem to be among the top priorities for inclusion.

## Next steps

- Calibrate the model
- Validate the model with independent datasets (different periods/seasons and other locations)

## References

- *microcimf* model by Ilya Maclean
- *SCOPE 2.0* model by Wim Verhoef & Christiaan van der Tol
- *ED 2.2* model by the *ED 2.2* development team

Table 2: Model parameters

name	explanation	U(min, max)	unit	submodel
$K_{b-v}$	direct beam radiation extinction coefficient in vertical direction	[0.5, 2]		
$K_{d-v}$	diffuse radiation extinction coefficient in vertical direction	[0.6, 0.95]		
$K_{b-h}$	direct beam radiation extinction coefficient in lateral direction	[0.3, 2]	unitless	SW RTM
$K_{d-h}$	diffuse radiation extinction coefficient in lateral direction	[0.5, 0.95]		
$\beta_0$	fraction of scattered direct beam radiation in backward direction	[0.2, 0.45]		
$\beta$	fraction of scatterd diffuse radiation in backward direction	[0.3, 0.35]		
$\omega$	shortwave scattering coefficient	[0.43, 0.61]		
$\omega_{g-v}$	shortwave ground scattering	[0.08, 0.18]		
$\omega_{g-h}$	shortwave scattering by the inner forest	[0.1, 0.2]		
$\epsilon_f$	emissivity of the forest	[0.94, 0.99]		
$K_{l-v}$	longwave radiation extinction coefficient in vertical direction	[0.2, 0.4]	unitless	LW RTM
$K_{l-h}$	longwave radiation extinction coefficient in lateral direction	[0.2, 0.4]		
$\beta_l$	fraction of scatterd longwave radiation in backward direction	[0.3, 0.35]		
$\omega_l$	longwave scattering coefficient	[0.01, 0.06]		
$\omega_{lg-v}$	longwave ground scattering	[0.04, 0.07]		
$\omega_{lg-h}$	longwave scattering by the inner forest	[0.01, 0.06]		
$h$	diffusion coefficient of air	[0, 20]	$W/m^2/K$	H
$p$	fraction of net radiation at ground level to define ground heat flux	[0.1, 0.35]	unitless	G
$g_s$	convection coefficient between air and soil surface	[5, 15]	$W/m^2/K$	$T_{air}$
$g_f$	convection coefficient between air and forest structure	[5, 20]	$W/m^2/K$	$T_{air}$ & H
$g_m$	convection coefficient between air and macroenvironment	[10, 40]	$W/m^2/K$	$T_{air}$
$i_s$	distance over which the influence of $T_s$ on $T_{air}$ is reduced bij 50%	[0, 10]	m	$T_{air}$
$i_f$	distance over which the influence of $T_f$ on $T_{air}$ is reduced bij 50%	[0, 10]	m	$T_{air}$
$i_m$	distance over which the influence of $T_{macro}$ on $T_{air}$ is reduced bij 50%	[5, 60]	m	$T_{air}$
$k_s$	thermal conductance of the soil	[0.25, 2.2]	$W/m/K$	$T_s$

Table 3: Input drivers (and spacetime specifics)

name	explanation	example value	unit
$T_{macro}$	macrotemperature at top canopy	31	°C
$T_{soil}$	soil temperature at 6cm depth	17	°C
$I_{sky,b}^\downarrow$	downward direct beam radiation at top canopy	600	$W/m^2$
$I_{sky}^\downarrow$	downward diffuse radiation at top canopy	200	$W/m^2$
$L_{sky}^\downarrow$	downward longwave radiation at top canopy	400	$W/m^2$
$\rho$	voxelised density from TLS point cloud	0.5	unitless
lat	latitude of forest site	50.980	°
long	longitude of forest stite	3.816	°
datetime	date & time of simulation/observation	2023-07-08 12:00:00	UTC

Table 4: (Physical) constants

name	explanation	value	unit	submodel
$\sigma$	Stefan-Boltzmann constant	5.67e-8	$W/m^2/K^4$	LW RTM
voxel size	length of the edge of a voxel cube	1	$m$	H
$c_p$	specific heat of air	1000	$J/kg/K$	H
$\rho_{air}$	air density	1.225	$kg/m^3$	H
$\alpha$	Priestley-Taylor coefficient	1.26	unitless	LE
$\gamma$	psychrometric constant	0.066	$kPa/K$	LE

Table 5: Prognostic variables (model outputs)

These outputs are modelled for each voxel at the steady state.

name	explanation	example value	unit
$T_f$	temperature of forest structure	28	°C
$T_s$	temperature of soil surface	21	°C
$T_{air}$	temperature of forest air	25	°C
$R_n$	net radiation flux	20	$W/m^2$
$H$	sensible heat flux	20	$W/m^2$
$LE$	latent heat flux	20	$W/m^2$
$G$	ground heat flux	20	$W/m^2$
$I_b^\downarrow$	downward direct beam radiation flux	20	$W/m^2$
$I^\downarrow$	downward diffuse radiation flux	20	$W/m^2$
$I^\uparrow$	upward diffuse radiation flux	20	$W/m^2$
$L^\downarrow$	downward longwave radiation flux	20	$W/m^2$
$L^\uparrow$	upward longwave radiation flux	20	$W/m^2$